Multiparametric modelling of composite materials based on non-intrusive PGD informed by multiscale analyses: application for real-time stiffness prediction of woven composites

M. El Fallaki Idrissi[a,b], F. Praud[a], V. Champaney[b], F. Chinesta[b], F. Meraghni[a,*]

[a] *Arts et Métiers Institute of Technology, CNRS, LEM3-UMR 7239, 4 rue Augustin Fresnel, 57078 Metz, France*
[b] *ESI Chair, Arts et Métiers Institute of Technology, CNRS, PIMM-UMR 8006, 151 Boulevard de l'Hôpital, 75013 Paris, France.*

Abstract

In this paper, a multiparametric solution of the stiffness properties of woven composites involving several microstructure parameters is performed. For this purpose, non-intrusive PGD-based methods are employed. From *offline* pre-computed solutions generated through a full-field multiscale modeling, the proposed method approximates the multidimensional solution as a sum of products of one-dimensional functions each depending on a single variable. The present work aims at providing an accurate approximation of this multiparametric solution with lower computational cost for dataset generation. Thus, a comparative analysis of three non-intrusive PGD formulations (SSL, s-PGD and ANOVA-PGD) is carried out. The obtained results reveal and demonstrate that the ANOVA-PGD model works well for approximating the

*Corresponding author. Arts et Métiers Institute of Technology, CNRS, LEM3-UMR 7239, 4 rue Augustin Fresnel, 57078 Metz, France
Email address: fodil.meraghni@ensam.eu (F. Meraghni)

stiffness properties over the entire parameter space, *i.e.*, along its boundary as well as inside it, by using only few pre-computed high-fidelity solutions. Finally, a GUI application is developed to exploit this multiparametric solution by incorporating other composite weave architectures. This application could be easily used by engineers and composite designers, to deduce, in real-time, the macroscopic properties of woven composite for a given set of microstructural parameters by simply varying the cursors and without any microstructure generation and meshing nor FE computations using periodic homogenization.

Keywords: woven composite material, multiscale modeling, geometrical and material parameters, non-intrusive PGD, multiparametric solution, mechanical properties.

Introduction

Textile-reinforced composites have been extensively used in a wide variety of industrial applications, including aerospace, automotive and many other engineering technologies due to their high stiffness-to-weight ratio, their impact resistance and their reduced production cost (Kumar, 2013; Long, 2006). This significant increase in the use of textile composites has created a strong demand not only to study their behavior under different loading conditions, but also to evaluate the impact of certain factors on their overall response. This can be achieved through experimental work or numerical studies, as has been already presented in several works (Hallal et al., 2013; Tikarrouchine et al., 2021; Miqoi et al., 2021; Zhou et al., 2021). However, numerical simulations offer a deep understanding of the stress-strain response and provide

more detailed information about the behavior and the associated mechanisms which is sometimes difficult to achieve using experiments.

The multiscale modeling approach has been shown to be effective to model the composite's behavior due to their ability to consider microscopic heterogeneities and to separate the problem into several tasks by modeling each phenomenon at the most relevant scale. Such implementation has been employed into linear as well as highly non-linear behavior modeling including viscoelasticity, viscoplasticity and damage (Tikarrouchine et al., 2018; Praud et al., 2017b). In general, this approach can be classified into two main categories. The first one is based on the so-called mean-field approaches, which are founded on Eshelby's equivalent inclusion theory (Eshelby, 1957), such as self-consistent method (Hill, 1965; Mercier and Molinari, 2009) and Mori-Tanaka scheme (Mori and Tanaka, 1973), for which further developments and computational approaches can be found in (Barral et al., 2020; Chen et al., 2022; Chatzigeorgiou et al., 2022). This first type allows deriving the macroscopic fields by averaging the same quantities of each material phase at the microscopic scale. Additionally, this approach is characterized by a fast computation cost but a limited accuracy especially when the matrix phase requires a nonlinear behavior. The second approach is well-known as full-field methods in which the homogenization process is performed using Finite Element (Chatzigeorgiou et al., 2016; Tikarrouchine et al., 2019; Praud et al., 2021a), Boundary Element (Kamiński, 1999), Finite Volume (Chen et al., 2018; de Sousa Vieira and Marques, 2019) and Fast Fourier Transformation based-homogenization techniques (Brisard and Dormieux, 2010; Wang et al., 2018), etc. Compared to semi-analytical models, full-field approaches gen-

erally provide better predictions of the stress-strain behavior of composites, but they are computationally expensive.

It is obvious that woven-fabric composites response is considerably affected by various factors that can be defined at different stages including the properties of constitutive phases and manufacturing parameters. Therefore, understanding the influence of these factors on the macroscopic properties of textile-reinforcement composites is of tremendous importance for more efficient employ of these materials according to the application needs. Several studies have been conducted over the past decades to investigate this impact on the homogenized properties of various textile composites, including woven composites that are manufactured by weaving process. Recently, the influence of yarn's angle on the local as well as on global behavior of woven composite, which can be induced by the manufacturing process such as shaping or performing, has been investigated in (Liang et al., 2020, 2019). In (Erol et al., 2017), the impact of yarn properties and weave architecture on the macroscopic response of 2D woven fabric composites have been studied.

Nevertheless, correctly defining the optimal choice of these parameters remains a challenging task especially for this class of composite due to the large number of the microstructural parameters and the related combinations that should be taken into account, leading hence to prohibitive cost of numerical simulation and to numerous experimental characterization. Thus, a Model Order Reduction (MOR) technique such as Proper Generalized Decomposition (PGD) is required, specifically, when many parameters are manipulated and a fast calculation is required for a real-time decision during the pre-desing or materials selection stages.

Based on the separated form of the unknown field, Proper Generalized Decomposition has become one of the most efficient approaches of MOR dealing with *the curse of dimensionality* (Ammar et al., 2006, 2007; Chinesta et al., 2010, 2011b,a). PGD has been used in different multiparametric problems involved in science and engineering fields, by assuming each parameter as an extra-coordinate of the problem. It has led to construct computational vademecum and virtual charts allowing the optimization and real-time simulation of complex problems (Chinesta et al., 2013; Ammar et al., 2014; Courard et al., 2016; Lu et al., 2018; Sancarlos et al., 2021b). This is achieved by providing, once and for all, in an *offline* stage, a global solution involving all the variables, *e.g.*, space, time and parameters, to later access, *on the fly*, to the solution for any new parameter instance, in an *online* phase. However, due to its *a priori* formulation, this approach is considered very intrusive to be implemented into industrial applications that utilize commercial software. Therefore, several studies have been conducted to circumvent or avoid the above difficulty by constructing the multidimensional solution in a non-intrusive manner (Germoso et al., 2020; Leon et al., 2019; Zou et al., 2018). As a possible way to minimize this implementation effort, some authors have proposed to pre-compute the high-fidelity solution for a set of parameter values, in order to interpolate them later using the separated representation of the parametric solution (Borzacchiello et al., 2019; Ibáñez et al., 2018; Sancarlos et al., 2021a). Other works have focused on coupling the commercial software with an external code that performs the decomposition as well as the assembly of the global solution using classical PGD framework (Zou et al., 2018).

Despite the recent parametric studies of woven composites, most of them do not perform a global solution in which we can get the engineering properties for any set of parameter values without repeating the multiscale computation. In this work, with the help of non-intrusive PGD-based methods, a multiparametric solution of the overall mechanical properties of woven composite is performed involving ten parameters chosen at different scales. More specifically, the aim is to achieve an accurate approximation of this multiparametric solution using few high fidelity solutions. Thus, three non-intrusive PGD formulations have been applied and compared to each other in order to obtain a trade-off between accuracy and the amount of data generated in the *offline* phase. This multiparametric approximation could then be used for real-time prediction of the overall mechanical properties of woven composites when the value of one or more inputs changes without going through multiscale computations. It might be employed as a decision tool to select the best material configuration for a specific application in terms of stiffness or overall response. It can also be useful for solving inverse design problems in which we can get the microstructure characteristics of the composite material with a given set of desired macroscopic effective properties.

The remainder of this paper is arranged as follows: in Section 1.1, a set of microstructural parameters which has an impact on the mechanical properties of woven composite, is presented. The creation of the microstructure and the mesh generation process are detailed in Section 1.2. Therefore, the multiscale modeling approach based on the periodic homogenization is briefly reviewed in Section 1.3. In Section 2, the theoretical background of three non-intrusive PGD techniques, *i.e.*, Sparse Subspace Learning (SSL),

Sparse Proper Generalized Decomposition (s-PGD) and ANOVA-PGD has been introduced. The last Section presents a comparative analysis of these techniques in terms of accuracy as well as the amount of data generated in the *Offline* stage.

1. Parametric computational homogenization for woven composites

1.1. Parametric representation

Woven composites are known to exhibit a complex anisotropic behavior arising from the geometrical arrangement of their microstructure along with the properties of their constituents, namely the woven reinforcement and the matrix. Classical woven reinforcements are usually obtained from an orthogonal interlacing of weft and warp yarns themselves composed of numerous fibres oriented along the 1^{st} and 2^{nd} directions, respectively. Several weaving patterns of woven fabrics are commonly employed in various industrial applications such as plain weave, twill weave (balanced/unbalanced) or satin weave. They are not characterized only by their different ways of weaving but also by their distinct features like stability, drape and smoothness. Therefore, the mechanical properties of woven composites are significantly affected by their microstructure and different macroscopic responses can be obtained by changing the geometry of the fabric reinforcement and the weaving pattern as well as the properties of the constituents and their nature (glass, carbon reinforcement, thermoplastic, thermoset or ceramic matrix, ...).

The present work focuses on woven composites with plain weave reinforcements, which are obtained by passing each weft yarn over and under each

warp yarn, with each row alternating. Based on this architecture, Figure 1 shows that the microstructure geometry and the properties of its constituents are defined by a set of ten independent parameters that represents: the fibre Young's modulus E_f, the fibre Poisson's ratio ν_f, the matrix Young's modulus E_m, the matrix Poisson's ratio ν_m, the weft intra-yarn fibre volume fraction c_{f1}, the warp intra-yarn fibre volume fraction c_{f2}, the weft yarn width a_1, the warp yarn width a_2, the gap between two adjacent yarns c and the fabric thickness h. Note that the gap between two adjacent yarns c is considered to be the same for the weft and warp yarns. Moreover, both yarns are also assumed to have a thickness equal to one half of the fabric thickness h, whereas 10% of h is added to define the matrix domain's thickness.

All these parameters are set in a vector $\boldsymbol{p} = \{p_1 \ p_2 \ \cdots \ p_{10}\}^{\mathrm{T}}$ whose members contain each one of the previously mentioned quantities as listed in Table 1. Each one of these parameters is associated with a range of values set between a minimum and maximum. All of theses ranges define the boundary of the 10-dimensional parametric space $\Omega_{\boldsymbol{p}} = \Omega_{p_1} \times \Omega_{p_2} \times \cdots \times \Omega_{p_{10}}$, covering a wide spectrum of woven composites that are commonly encountered in engineering applications, such as glass or aramid fibres with epoxy or polyester matrices, or many other configurations.

It is worthwhile to mention that, although the yarns are composed of numerous unidirectionally oriented fibres embedded in the matrix, as shown in Figure 1a. They are considered in the present approach as an equivalent transversely isotropic homogeneous medium whose apparent stiffness properties are analytically calculated by means of the well-known Mori-Tanaka sheme (*Micro-homogenization*), from the fibres and matrix prop-

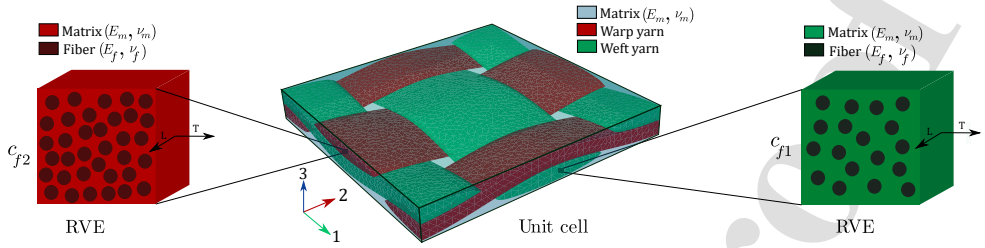

(a) Material parameters of the microstructure.

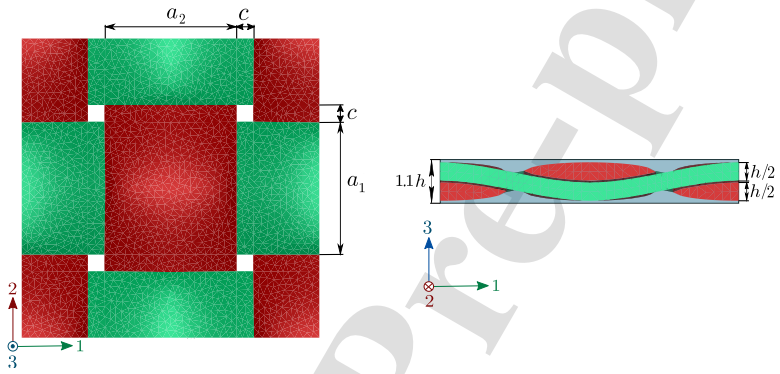

(b) Geometric parameters of the microstructure.

Figure 1: Parametric representation of the microstructure of the woven composite. (a) Material parameters of the microstructure, namely: the fibre Young's modulus E_f, the fibre Poisson's ratio ν_f, the matrix Young's modulus E_m, the matrix Poisson's ratio ν_m, the weft intra-yarn fibre volume fraction c_{f1} and the warp intra-yarn fibre volume fraction c_{f2}. The apparent stiffness properties of the yarns are analytically calculated from the fibres and matrix properties, namely: E_f, ν_f, E_m and ν_m, as well as c_{f1} and c_{f2}. (b) Geometric parameters of the microstructure, namely: the weft yarn width a_1, the warp yarn width a_2, the gap between two adjacent yarns c and the fabric thickness h.

erties, namely: E_f, ν_f, E_m and ν_m, as well as the intra-yarn fibre volume fractions c_{f1} and c_{f2}. Therefore, this results in five independent elastic constants for the yarn, namely: E_L^k, E_T^k, G_{LT}^k, ν_{LT}^k and ν_{TT}^k, where the subscript L and T denote the longitudinal and transverse directions, whereas the su-

Table 1: Microstructural parameters of the woven composite. Each one of these parameters is associated with a range of values set between a minimum and maximum, covering a wide spectrum of woven composites that are commonly encountered in engineering applications.

Parameter	Description	Min. value	Max. value	unit
p_1	Fibre Young's modulus E_f	50 000	100 000	MPa
p_2	Fibre Poisson's ratio ν_f	0.2	0.4	-
p_3	Matrix Young's modulus E_m	500	5 000	MPa
p_4	Matrix Poisson's ratio ν_m	0.2	0.4	-
p_5	Weft intra-yarn fibre volume fraction c_{f1}	0.3	0.7	-
p_6	Warp intra-yarn fibre volume fraction c_{f2}	0.3	0.7	-
p_7	Weft yarn width a_1	0.8	4.5	mm
p_8	Warp yarn width a_2	0.8	4.5	mm
p_9	Gap between two adjacent yarns c	0.1	0.4	mm
p_{10}	Fabric thickness h	0.2	0.6	mm

perscript $k = 1, 2$ stands for the weft and warp yarns, respectively.

1.2. Mesh generation of the unit-cell

To perform computational homogenization on woven composites, a finite element mesh of the composite unit-cell, which represents the smallest repetitive unit element of the microstructure, is required. Many works have been undertaken to deal with the microstructure generation of woven composites, leading to the development of several dedicated tools, such as *WiseTex* (Verpoest and Lomov, 2005) or *TexGen* (Lin et al., 2011). In the present work, a python script attached to the software *TexGen* is developed to automatically generate a finite element mesh of the woven unit-cell for a given set of geometrical parameters (p_7, p_8, p_9, p_{10}). Figure 2 shows some examples of unit-cell's mesh generated by the developed python script and *TexGen* for arbitrary sets of parameters.

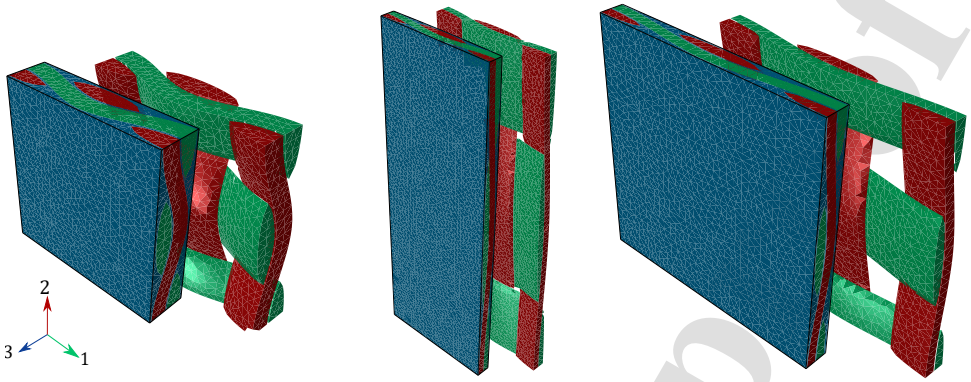

Figure 2: Examples of unit cell (The entire unit cell and the Yarns) that can be generated through *TexGen* by varying different geometrical parameters for instance the weft yarn width a_1, the warp yarn width a_2, the gap between two adjacent yarns c and the fabric thickness h)

It is worth noticing that the yarn are transversely isotropic and therefore their behavior strongly depends on a certain material orientation, which is defined in each yarn element in such a way that the fibre direction L is always oriented along the middle line of the yarns.

1.3. Computational homogenization

When considering a full-field multiscale approach such as periodic homogenization, it is essential to define a proper connection between the microscopic and macroscopic scales. This connection is usually established by averaging the microscopic stress and strain over the unit-cell's domain $\mathfrak{B}$ (Hill, 1967; Mura, 2013; Nemat-Nasser and Hori, 2013). Accordingly, it yields for the macroscopic stress and strain:

$$\overline{\boldsymbol{\sigma}} = \frac{1}{V} \int_{\mathfrak{B}} \boldsymbol{\sigma}(\boldsymbol{x}) \, \mathrm{d}V, \tag{1a}$$

$$\overline{\boldsymbol{\varepsilon}} = \frac{1}{V}\int_{\mathfrak{B}} \boldsymbol{\varepsilon}(\boldsymbol{x})\ \mathrm{d}V, \tag{1b}$$

respectively, where V represents the volume of the unit-cell's domain $\mathfrak{B}$.

Within the unit-cell, the assumption of periodicity implies that it yields for the displacement $\boldsymbol{u}$, the following additive form:

$$\boldsymbol{u}(\boldsymbol{x}) = \overline{\boldsymbol{\varepsilon}} \cdot \boldsymbol{x} + \boldsymbol{u}'(\boldsymbol{x}) + \boldsymbol{u}_0, \qquad \forall \boldsymbol{x} \in \mathfrak{B} \tag{2}$$

where the first term, *i.e.*, $\overline{\boldsymbol{\varepsilon}} \cdot \boldsymbol{x}$ depicts an affine part, the second term, *i.e.*, $\boldsymbol{u}'$ stands for a periodic fluctuation, while $\boldsymbol{u}_0$ represents an eventual rigid body motion. Since $\boldsymbol{u}'$ is a periodic function, it takes the same values at each pair of opposite points $\boldsymbol{x}_+$ and $\boldsymbol{x}_-$ on the unit-cell's border $\partial\mathfrak{B}$:

$$\boldsymbol{u}'(\boldsymbol{x}_+) = \boldsymbol{u}'(\boldsymbol{x}_-), \qquad \forall \boldsymbol{x}_+, \boldsymbol{x}_- \in \partial\mathfrak{B} \tag{3}$$

Moreover, due to its periodic aspect, the part of the strain produced by $\boldsymbol{u}'$ vanishes once averaged, which renders the whole strain average well equal to the macroscopic strain as expressed in (1b). By inserting (2) into (3), the periodicity conditions can be reformulated in terms of $\boldsymbol{u}$ instead of $\boldsymbol{u}'$, while involving the macroscopic strain tensor $\overline{\boldsymbol{\varepsilon}}$:

$$\boldsymbol{u}(\boldsymbol{x}_+) - \boldsymbol{u}(\boldsymbol{x}_-) = \overline{\boldsymbol{\varepsilon}} \cdot (\boldsymbol{x}_+ - \boldsymbol{x}_-), \qquad \forall \boldsymbol{x}_+, \boldsymbol{x}_- \in \partial\mathfrak{B} \tag{4}$$

which represents the Periodic Boundary Conditions (PBCs) applied to the unit-cell. Therefore, the PBCs enable setting any macroscopic strain state to the unit-cell whereas the macroscopic stress can be recovered through the scale transition relationship (1a) once the unit-cell problem solved. From a practical point of view, when used in the finite element method, the PBCs are applied to meshed unit-cell by introducing the six components of $\overline{\boldsymbol{\varepsilon}}$ as

additional degrees of freedom that are connected to the unit-cell's borders through kinematic constraint equations. For more details regarding this aspect, readers are referred to (Michel et al., 1999; Praud, 2018).

In the context of linear elasticity, the macroscopic stiffness tensor $\overline{\mathbb{C}}$ can be recovered through a perturbation analysis, *i.e.*, by computing the macroscopic stress resulting from the six elementary macroscopic strain states. With the help of the Voigt notation, it yields for the elementary strain states:

$$\begin{cases} \overline{\boldsymbol{\varepsilon}}_{(11)} = \left\{\overline{\varepsilon}_{11}=\delta \quad \overline{\varepsilon}_{22}=0 \quad \overline{\varepsilon}_{33}=0 \quad 2\overline{\varepsilon}_{12}=0 \quad 2\overline{\varepsilon}_{13}=0 \quad 2\overline{\varepsilon}_{23}=0\right\}^{\mathrm{T}} \\ \overline{\boldsymbol{\varepsilon}}_{(22)} = \left\{\overline{\varepsilon}_{11}=0 \quad \overline{\varepsilon}_{22}=\delta \quad \overline{\varepsilon}_{33}=0 \quad 2\overline{\varepsilon}_{12}=0 \quad 2\overline{\varepsilon}_{13}=0 \quad 2\overline{\varepsilon}_{23}=0\right\}^{\mathrm{T}} \\ \overline{\boldsymbol{\varepsilon}}_{(33)} = \left\{\overline{\varepsilon}_{11}=0 \quad \overline{\varepsilon}_{22}=0 \quad \overline{\varepsilon}_{33}=\delta \quad 2\overline{\varepsilon}_{12}=0 \quad 2\overline{\varepsilon}_{13}=0 \quad 2\overline{\varepsilon}_{23}=0\right\}^{\mathrm{T}} \\ \overline{\boldsymbol{\varepsilon}}_{(12)} = \left\{\overline{\varepsilon}_{11}=0 \quad \overline{\varepsilon}_{22}=0 \quad \overline{\varepsilon}_{33}=0 \quad 2\overline{\varepsilon}_{12}=\delta \quad 2\overline{\varepsilon}_{13}=0 \quad 2\overline{\varepsilon}_{23}=0\right\}^{\mathrm{T}} \\ \overline{\boldsymbol{\varepsilon}}_{(13)} = \left\{\overline{\varepsilon}_{11}=0 \quad \overline{\varepsilon}_{22}=0 \quad \overline{\varepsilon}_{33}=0 \quad 2\overline{\varepsilon}_{12}=0 \quad 2\overline{\varepsilon}_{13}=\delta \quad 2\overline{\varepsilon}_{23}=0\right\}^{\mathrm{T}} \\ \overline{\boldsymbol{\varepsilon}}_{(23)} = \left\{\overline{\varepsilon}_{11}=0 \quad \overline{\varepsilon}_{22}=0 \quad \overline{\varepsilon}_{33}=0 \quad 2\overline{\varepsilon}_{12}=0 \quad 2\overline{\varepsilon}_{13}=0 \quad 2\overline{\varepsilon}_{23}=\delta\right\}^{\mathrm{T}} \end{cases}, \tag{5}$$

where δ is a real value. The simplest way is to take $\delta = 1$. Figure 3 shows, for one example of generated woven composite unit-cell, the deflection modes obtained for each of these elementary macroscopic strain states. Thus, the C_{ijkl} component of the macroscopic stiffness tensor $\overline{\mathbb{C}}$ can be recovered by computing the ij component of the stress tensor obtained for the kl elementary strain state, divided by δ:

$$\overline{C}_{ijkl} = \frac{\overline{\sigma}_{ij(kl)}}{\delta} \qquad ij, kl = 11, 22, 33, 12, 13, 23 \tag{6}$$

The arrangement of the woven microsructure leads to orthotropic stiffness properties such that $\overline{\mathbb{C}}$ can be expressed from nine independent elastic constants, namely: $\overline{E}_1$, $\overline{E}_2$, $\overline{E}_3$, $\overline{G}_{12}$, $\overline{G}_{13}$, $\overline{G}_{23}$, $\overline{\nu}_{12}$, $\overline{\nu}_{13}$ and $\overline{\nu}_{23}$, according to

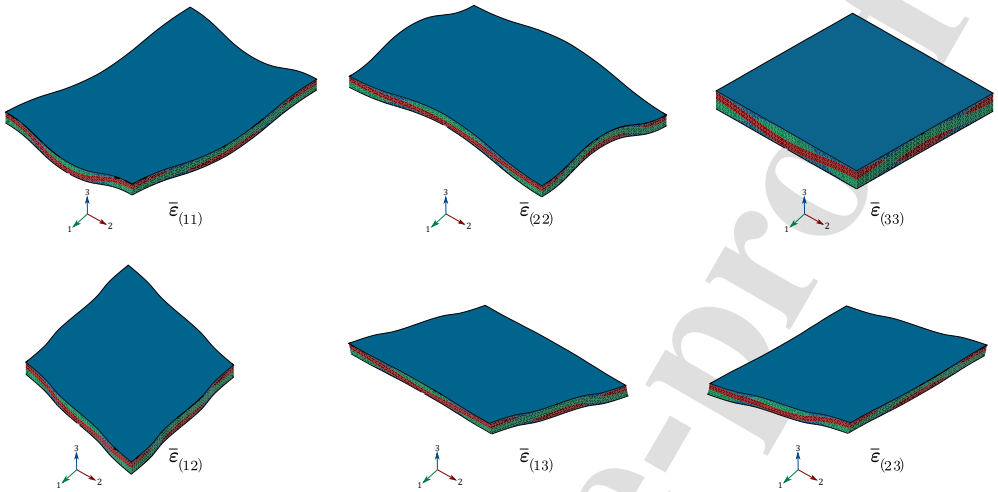

Figure 3: Deflection modes of the unit cell for each of the elementary macroscopic strain states $\overline{\boldsymbol{\varepsilon}}_{(11)}$, $\overline{\boldsymbol{\varepsilon}}_{(22)}$, $\overline{\boldsymbol{\varepsilon}}_{(33)}$, $\overline{\boldsymbol{\varepsilon}}_{(12)}$, $\overline{\boldsymbol{\varepsilon}}_{(13)}$, and $\overline{\boldsymbol{\varepsilon}}_{(23)}$.

the following relationship:

$$\overline{\mathbb{C}}^{-1} = \begin{pmatrix} \frac{1}{\overline{E}_1} & -\frac{\overline{\nu}_{12}}{\overline{E}_1} & -\frac{\overline{\nu}_{13}}{\overline{E}_1} & 0 & 0 & 0 \\ & \frac{1}{\overline{E}_2} & -\frac{\overline{\nu}_{23}}{\overline{E}_2} & 0 & 0 & 0 \\ & & \frac{1}{\overline{E}_3} & 0 & 0 & 0 \\ & & & \frac{1}{\overline{G}_{12}} & 0 & 0 \\ & & & & \frac{1}{\overline{G}_{13}} & 0 \\ \text{sym.} & & & & & \frac{1}{\overline{G}_{23}} \end{pmatrix} \tag{7}$$

Therefore, based on the above equation, the elastic constants of the woven composite are identified from the computed stiffness tensor. They are afterwards stored in an output vector $\boldsymbol{w}$:

$$\boldsymbol{w} = \{\overline{E}_1\ \overline{E}_2\ \overline{E}_3\ \overline{G}_{12}\ \overline{G}_{13}\ \overline{G}_{23}\ \overline{\nu}_{12}\ \overline{\nu}_{13}\ \overline{\nu}_{23}\}^{\mathrm{T}} \tag{8}$$

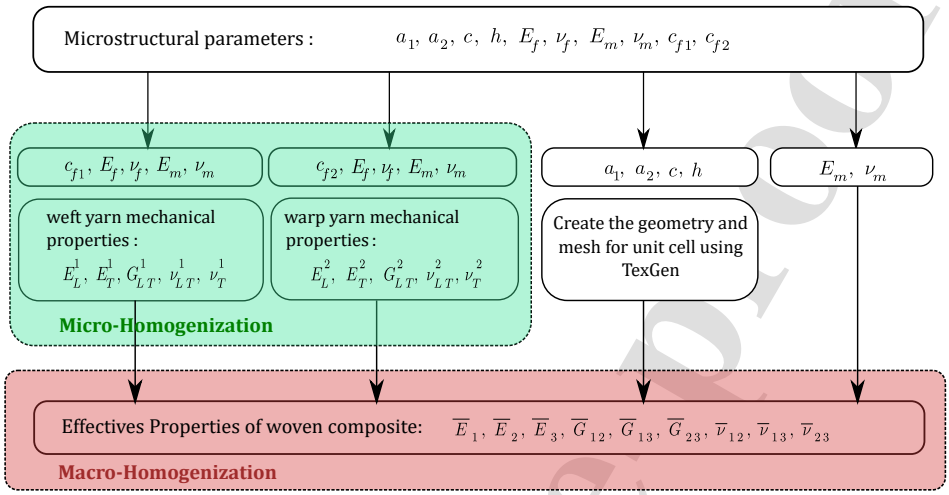

Figure 4: Schematic illustration of data generation process using multiscale modeling, from microstructural parameters (input values) to the overall mechanical properties of woven composite (output values).

2. Non-intrusive PGD

As summarized in Figure 4, the estimation of the macrospcopic stiffness properties of woven composites depends on a numerical process involving homogenization techniques as well as the use of several software like *TexGen* and a finite element solver, *Abaqus/Standard* in the present case. Although, this numerical process is relatively quick and can easily be automated, a few dozen of minutes are still necessary to obtain a result. Such a computational cost is sufficiently important to hamper its use towards for simulation-based engineering, which may be limited in some way by the need to evaluate several configurations for different parameter values in order to achieve a satisfactory solution. This can make the design and the optimization process very time consuming. To overcome these limitations, it is proposed to use the concept of

non-intrusive PGD to set up a multiparametric approximation based on pre-computed solutions at certain points of the parametric space. Non-intrusive PGD methods are particularly convenient for this purpose as it only employs data that may be independently obtained from standard numerical processes, *e.g.*, finite element simulations. This is in contrast with classical PGD-based methods that require specifically adapted numerical processes or solvers. The main idea behind such as technique is to approximate the solution as a finite sum of products of one-dimensional functions :

$$w(p_1, ..., p_N) \approx \sum_{i=1}^{M} \prod_{j=1}^{N} W_j^i(p_j) \tag{9}$$

where N and M refer to the number of variables and the number of modes (the terms of the sum), respectively, while W_j^i denotes a one-dimensional function that depends only on the variable p_j. For the reader interested in PGD-based approaches, more accurate information could be found in (Chinesta et al., 2011b,a) and the references therein.

In this work, three non-intrusive PGD techniques have been investigated and evaluated to obtain an accurate approximation of the parametric solution using lower computational cost in the *offline* step. Indeed, Sparse Subspace Learning (SSL) (Borzacchiello et al., 2019), Sparse Proper Generalized Decomposition (s-PGD) (Ibáñez et al., 2018) and ANOVA-PGD (Sancarlos et al., 2021a) have been performed and compared in terms of accuracy and robustness. They are used to predict the mechanical properties of 2D woven composite taking into account the microstructural parameters listed above.

2.1. Sparse Subspace Learning (SSL)

Sparse Subspace Learning (SSL) consists in using a hierarchical basis in a sparse grid space to approximate the unknown solution. It utilizes the Gauss-Lobatto-Chebychev collocation points $\boldsymbol{p}^{i(k)} = (p_1^{i(k)}, ..., p_{10}^{i(k)})$ associated with polynomial function $\zeta_j^{i(k)}$, where i denotes the point index, k refers to the level of approximation and j represents the variable index. It is used here to approximate each component w of the nine mechanical properties of woven composite.

At the first level (k=0), each component w can be approximated from w_0 using 2^{10}=1024 collocation points $\boldsymbol{p}^{i(0)} = (p_1^{i(0)}, ..., p_{10}^{i(0)})$, $i = 1, ..., 1024$:

$$w(p_1, ..., p_{10}) \approx w_0(p_1, ..., p_{10}) = \sum_{i=1}^{1024} \gamma_i \prod_{j=1}^{10} \zeta_j^{i(0)}(p_j) \tag{10}$$

where $\gamma_i = w(\boldsymbol{p}^{i(0)})$ represents the high fidelity solution of the woven composite obtained by the multiscale modeling at the collocation point $\boldsymbol{p}^{i(0)}$.

The one-dimensional function can be expressed using Lagrange polynomial as follows:

$$\zeta_j^{i(k)}(p_j) = \prod_{l \neq i} \frac{(p_j - p_j^{l(k)})}{(p_j^{i(k)} - p_j^{l(k)})} \tag{11}$$

where k refers to the level of approximation, j is the index variable and l refers to the index of the value of the parameter p_j. For instance, for the first level (k=0), $p_j^{l(0)}$ stands for the lower and upper bounds of the parameter p_j.

The process of enriching the approximation proceeds by adding surpluses to the solution as the hierarchical approximation level is raised. Therefore, at the second level (k=1), the approximation of w can be updated by adding more sampling points (5120 samples) and expressed as:

$$w(p_1, ..., p_{10}) \approx w_0(p_1, ..., p_{10}) + w_1(p_1, ..., p_{10}) \tag{12}$$

with w_1 is given by:

$$w_1(p_1, ..., p_{10}) = \sum_{i=1}^{5120} \tilde{\gamma}_i \prod_{j=1}^{10} \zeta_j^{i(1)}(p_j) \tag{13}$$

where $\tilde{\gamma}_i = w(\boldsymbol{p}^{i(1)}) - w_0(\boldsymbol{p}^{i(1)})$ is the gap between the predicted and reference values of the macroscopic property at the sampling point $\boldsymbol{p}^{i(1)}$. This gap is also called the surplus and its norm can be used as an error indicator to stop or continue the enrichment process.

It is worth noting that the current technique always guarantees an exact solution at all sampling points. Also, the enrichment process does not disturb this solution in the previous hierarchical levels. In other words, the approximate solution remains unaffected at the previous sampling points. Thus, at each level, the added term equals zero in all points that have been used in the preceding levels, for instance, at level 1, $w_1(\boldsymbol{p}^{i(0)}) = 0$. On the other hand, the improvement of the approximation requires a huge number of pre-computed solutions. Therefore, more than 15 000 collocation points are required to approximate the parametric solution at the 3^{rd} level.

2.2. Sparse Proper Generalized Decomposition (s-PGD)

Sparse Proper Generalized Decomposition is an alternative procedure for constructing a sparse approximation in a high-dimensional space from a limited dataset. It is developed to circumvent the drawbacks of the previous method by dealing with the *curse of dimensionality* as well as the non-structured datasets. It is also based on the concept of separate variables as depicted in Eq. (9).

As the problem under study involves ten parameters, it is assumed that the objective function $w_b(\boldsymbol{p})$ (corresponding to a macroscopic property) lives

in a 10-dimensional space $\Omega_{\boldsymbol{p}} = \Omega_{p_1} \times \cdots \times \Omega_{p_{10}} \subset \mathbb{R}^{10}$. Furthermore, it is assumed that the value of this mechanical property is known only at few locations where it is calculated numerically. In order to predict the mechanical properties of any new woven composite arrangement, without resorting to numerical computations, s-PGD provides thus an approximate solution w_p to the objective function using the PGD framework. For this reason, the Galerkin projection is chosen and the approximate solution is searched as follows:

$$\int_{\Omega_p} q^*(\boldsymbol{p})\Big(w_p(\boldsymbol{p}) - w_b(\boldsymbol{p})\Big)\mathrm{d}p_1 \cdots \mathrm{d}p_{10} = 0 \tag{14}$$

where $q^*(\boldsymbol{p}) \in \mathscr{C}^0(\Omega_p)$ is a test function. Since the solution is known only at few points, the test function q^* is defined as a set of Dirac delta functions located at the sampling points $\boldsymbol{p}^k = (p_1^k, ..., p_{10}^k)$, $k = 1, ..., P$, and given by the following relationship:

$$q^*(\boldsymbol{p}) = w^*(\boldsymbol{p}) \sum_{i=1}^{P} \delta(\boldsymbol{p}^k) \tag{15}$$

where P is the total number of sampling points. $\delta(\boldsymbol{p}^k)$ refers to the Dirac delta function that is null in the whole domain, except at the sampling points $\boldsymbol{p}^k$.

It is convenient to rewrite the Eq. (15) as:

$$q^*(\boldsymbol{p}) = (W_1^{M*} \cdots W_{10}^{M} + ... + W_1^{M} \cdots W_{10}^{M*}) \sum_{i=1}^{P} \delta(\boldsymbol{p}^k) \tag{16}$$

According to the PGD principle, w_p can be approximated as a sum of product of one-dimensional functions W_j^i which depends on the parameter p_j:

$$w_p(\boldsymbol{p}) \approx w^M(\boldsymbol{p}) = \sum_{i=1}^{M} \prod_{j=1}^{N=10} W_j^i(p_j) \tag{17}$$

where M refers to the number of modes and N represents the number of parameters.

w^M can also be expressed as follows:

$$w^M(\boldsymbol{p}) = w^{M-1}(\boldsymbol{p}) + \prod_{j=1}^{N=10} W_j^M(p_j) \tag{18}$$

where w^M and w^{M-1} represent the approximate solution using M and $M-1$ modes, respectively. It should be noted that only the functions W_j^M involved at mode M are assumed unknown, while w^{M-1} is considered to be known and expressed as follows :

$$w^{M-1}(\boldsymbol{p}) = \sum_{i=1}^{M-1} \prod_{j=1}^{N=10} W_j^i(p_j) \tag{19}$$

Following the PGD framework, a finite element projection is performed and a greedy algorithm is employed in order to compute these one-dimensional functions at the M-th mode. Since, these functions are expressed, in a general form, as follows:

$$W_j^M(p_j) = \sum_{k=1}^{D} \phi_k(p_j)\lambda_k = \mathbf{\Phi}_j^T \boldsymbol{\lambda}_j \tag{20}$$

where $\boldsymbol{\lambda}_j$ and $\mathbf{\Phi}_j^T$ refer to the vector of degrees of freedom and the shape functions that contained D components of the j-th dimension.

2.3. ANOVA-PGD

ANOVA decomposition is an orthogonal decomposition which can be used to approximate a multidimensional function w as a sum of numerous func-

tions .

$$w(\boldsymbol{p}) = w(p_1, ..., p_N) = w_\emptyset + \sum_{j_1=1}^{N} w_{j_1}(p_{j_1}) + \sum_{1 \leq j_1 < j_2 \leq N}^{N} w_{j_1,j_2}(p_{j_1}, p_{j_2}) + ... + w_{1,...,N}(p_1, ..., p_N) \tag{21}$$

Satisfying the expectation $\mathbb{E}_j$ with respect to j $(j_1, ..., j_{n \leq N})$:

$$\mathbb{E}_j(w_{j_1,...,j_n}(p_{j_1}, ..., p_{j_n})) = 0 \tag{22}$$

The anchored ANOVA decomposition is an alternative way to orthogonally decompose the solution w as a sum of functions defined with respect to an anchor point $\boldsymbol{p}_c = (p_1^c, ..., p_{10}^c)$. It allows to reduce the computational cost induced by the classical ANOVA decomposition. So, the constant term $w_\emptyset = w(\boldsymbol{p}_c)$ is determined by calculating the solution at anchor point $\boldsymbol{p}_c$ which is chosen here as being at center of the parametric domain.

ANOVA-PGD (Sancarlos et al., 2021a) consists of combining the anchored ANOVA decomposition with non-intrusive PGD, providing an accurate approximation of the multidimensional solution in low-data limit. First, the multidimensional solution is approximated using the anchored ANOVA decomposition. Then, based on one of the non-intrusive PGD techniques such as s-PGD, the solution is improved by approaching the residual as follows :

$$w_{\text{non-intrusive PGD}}(\boldsymbol{p}) \approx w(\boldsymbol{p}) - w_{\text{ANOVA}}(\boldsymbol{p}) \tag{23}$$

while the w_{ANOVA} is obtained, here, by using only the first terms of the sum (one-dimensional functions w_{j_1} which depend on the variable p_{j_1}) as :

$$w_{\text{ANOVA}}(\boldsymbol{p}) = w_\emptyset + \sum_{j_1=1}^{N=10} w_{j_1}(p_{j_1}) \tag{24}$$

where w_{j_1} can be expressed as following (For instance if $j_1 = 1$) :

$$w_1(p_1) = w_\emptyset + w(p_1, p_2^c, ..., p_N^c) \tag{25}$$

3. Results and discussion

In this section, a comparative analysis of these three non-intrusive PGD methods is discussed on three levels. Fist, a test dataset of 160 samples have been generated through multiscale modeling, as introduced earlier, to evaluate the performance of each model. The proposed 160 samples are divided into two equal parts for better interpretation of the results. The first set is represented by 80 pre-selected samples located inside the parametric domain and plotted in blue color, while the rest of the samples are taken on its boundary and depicted in red color, as shown in Figures 7, 5, 6 and 8. Second, one of the nine components of the mechanical properties (The Young's Modulus of the composite along the weft direction) is plotted by varying two of the most influential parameters on the elastic behavior of plain woven composite (fibre Young's modulus E_f and intra-weft fibre volume fraction c_{f1}), holding the remaining parameters at two positions ($a_1 = 2$ mm, $a_2 = 2$ mm, $h = 0.3$ mm, $c = 0.2$ mm, $c_{f2} = 50\%$, $v_f = 0.3$, $E_m = 2074$ MPa and $v_m = 0.3$) as depicted in Figure 9 and ($a_1 = 0.8$ mm, $a_2 = 0.8$ mm, $h = 0.2$ mm, $c = 0.1$ mm, $c_{f2} = 30\%$, $v_f = 0.2$, $E_m = 500$ MPa and $v_m = 0.2$) as shown in Figure 10. Finally, a quantitative comparison is presented in the Table 2, indicating the error obtained and the volume of data requested by each technique.

The error produced by each method in the test dataset is expressed as

follows:

$$E_{rr} = \frac{\sqrt{\sum_{k=1}^{T}\left(w(\boldsymbol{p}^k) - w_{app}(\boldsymbol{p}^k)\right)^2}}{\sqrt{\sum_{k=1}^{T}\left(w(\boldsymbol{p}^k)\right)^2}} \tag{26}$$

where $T = 160$ refers to the total number of test dataset. w and w_{app} represent the reference and the approximate solution of each mechanical property, respectively, at the test point $\boldsymbol{p}^k$.

3.1. Macroscopic properties predicted by SSL :

As has already been pointed out, the samples needed to construct the parametric solution with SSL model are typically acquired following the Sparse Grid Sampling strategy and based on Gauss-Lobatto-Chebyshev collocation points. It allows us to circumvent the overfitting problems induced by increasing the degree of the polynomials. Moreover, it involves a reduced volume of data at each level compared to the full sampling strategy. As a result, 1024 samples are used to approximate the solution at the first hierarchical level, which represent all possible combinations between the minimum and maximum values of the 10-dimensional space. Herein, due to this sampling strategy, only 16 unit-cells are sufficient to calculate the mechanical properties at all 1024 sampling points, as the samples may have the same unit-cell geometry (similar geometrical parameters: a_1, a_2, c, and h) but different constituent material properties (E_f, ν_f, E_m, etc). In addition, more sampling points could be added in the subsequent levels to improve the accuracy of the approximation. For instance, 5120 samples are required for level 1, including 32 unit-cells.

The macroscopic properties predicted using SSL level 0 and level 1 against

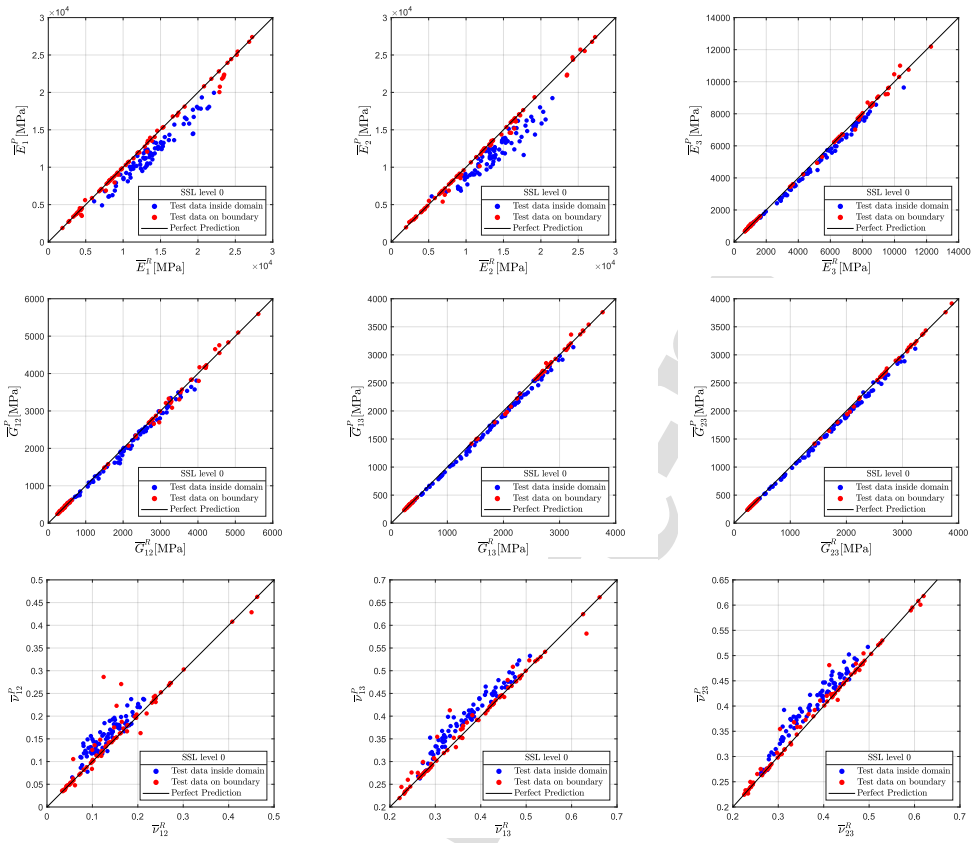

Figure 5: Scatterplots of the predicted values against the reference ones of the mechanical properties of plain weave fabric composite using SSL level 0. The red and blue points refer to the test datasets on boundary and inside the parametric domain, respectively. While the diagonal line indicate the perfect prediction.

the reference values for the test dataset are illustrated in Figures 5 and 6, respectively. In general, an excellent correlation between predicted and reference values can be observed from these figures, when the test sampling points are located on the boundary. Whereas, a large deviation of predicted mechanical properties from the diagonal line can be noticed for the dataset points inside the domain, especially for the Young modulus along the 1$^{\text{st}}$ and

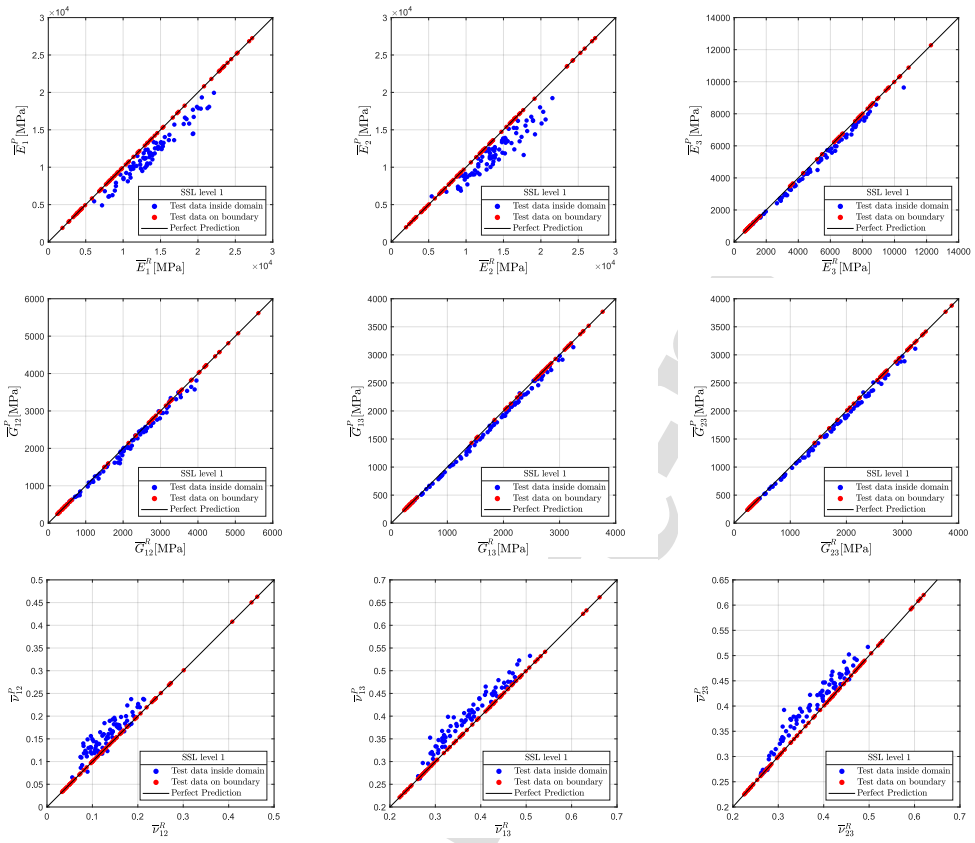

Figure 6: Scatterplots of the predicted values against the reference ones of the mechanical properties of plain weave fabric composite using SSL level 1. The red and blue points refer to the test datasets on boundary and inside the parametric domain, respectively. While the diagonal line indicate the perfect prediction.

2nd directions and the Poisson ratios.

Despite the increase in the number of sampling points from level 0 to level 1, we notice that there is not much difference between the scatterplots in Figure 5 and Figure 6, except for a few red points that have been now placed on the diagonal line. This means that the accuracy of the approximate solution does not improve significantly, even with the considerable increase in the

number of samples. Similar results can be clearly noticeable in Subfigures 9b, 9c, 10b and 10c where the predicted and reference values of the Young's Modulus along the direction 1 ($\overline{E}_1$) are plotted as a function of two parameters (E_f and c_{f1}), while the others are maintained constant and collected at two different locations (the center and the boundary of the parametric domain). The results obtained are first explained by the high concentration of sampling points along the domain boundary for both hierarchical levels. Second, the solution is quite smooth along the boundary and only a small variation is noticed inside the parametric domain. It should be noted that more accurate results could be found by having more knowledge about the solution in the middle of the parametric domain. This can be achieved by enriching more the approximation through the increase of the hierarchical levels (Ibáñez et al., 2018). However, this can be very time consuming due to the exponential expansion in sampling points. Furthermore, as summarized in Table 2, the SSL level 0 and 1 necessitate a few dozen of unit cell generations. Such a number still allows punctual corrections that are sometimes needed on some unit cells since the automatic generation does not always provide perfect meshes. This is in contrast with higher levels of approximation, which require too many unit cells (for instance, more than 100 for the level 2) to perform these corrections.

3.2. Macroscopic properties predicted by s-PGD

This model has been trained with 200 samples given by the Latin Hypercube Sampling (LHS) strategy. This strategy consists of generating points in a quasi-random way under the condition that only one sample is placed on the same row and column. That is why, generating a training dataset of 200

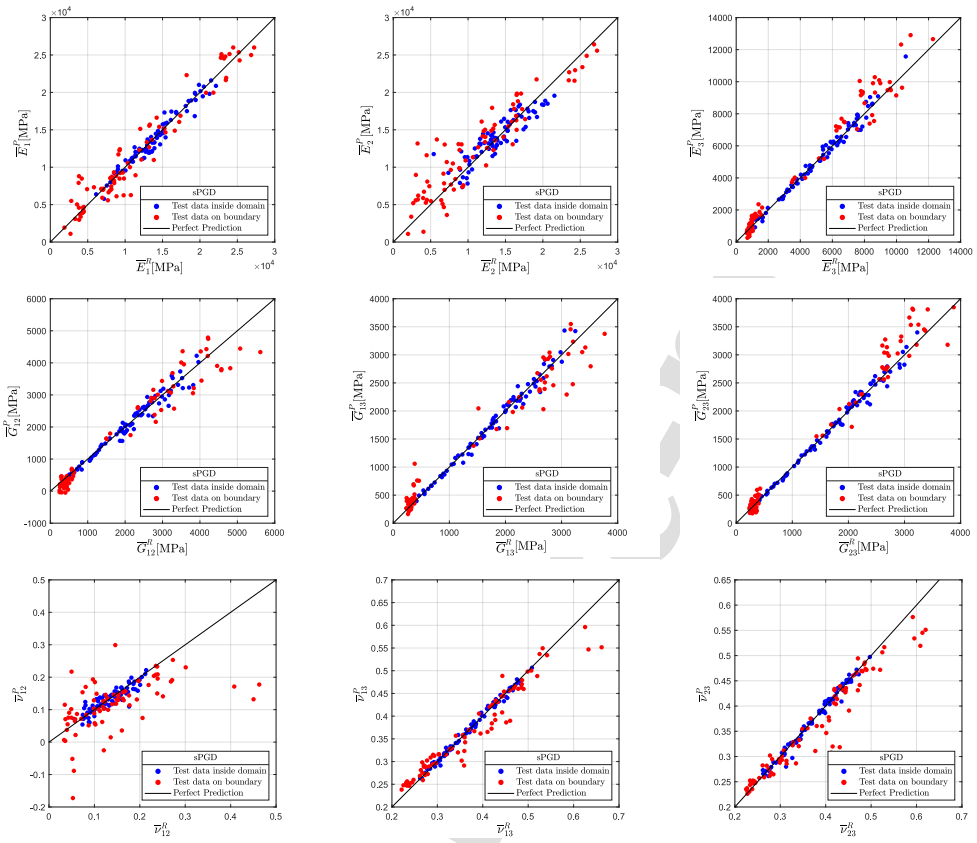

Figure 7: Scatterplots of predicted versus reference values of the mechanical properties of plain weave fabric composite using s-PGD model. The red and blue points represent the test datasets on boundary and inside the parametric domain, respectively. While the diagonal line indicate the perfect prediction.

samples, in this case, necessitates similar number of unit-cells. In addition, it should be noted that a hyperparametric study is conducted to identify the input values of the model's hyperparameters, such as the number of sampling points, the degree of the one-dimensional polynomial and the number of modes. Consequently, linear and quadratic polynomials are adopted and a mode number ranging between 10 and 16 are found for the nine components.

Therefore, for the same reasons as mentioned in the previous subsection, the database could not be improved with a higher number of sampling points, and the latter is set to 200 samples. This is particularly motivated by the large number of unit cells required for this sampling strategy.

The scatterplots obtained by comparing the reference values ($\overline{E}_1^R$, $\overline{E}_2^R$, $\overline{E}_3^R$, $\overline{G}_{12}^R$, $\overline{G}_{13}^R$, $\overline{G}_{23}^R$, $\overline{\nu}_{12}^R$, $\overline{\nu}_{13}^R$, $\overline{\nu}_{23}^R$) and the values predicted by the s-PGD model ($\overline{E}_1^P$, $\overline{E}_2^P$, $\overline{E}_3^P$, $\overline{G}_{12}^P$, $\overline{G}_{13}^P$, $\overline{G}_{23}^P$, $\overline{\nu}_{12}^P$, $\overline{\nu}_{13}^P$, $\overline{\nu}_{23}^P$) for the nine elastic constants are illustrated in Figure 7. It can be clearly observed from this figure that s-PGD provided a correct estimation of the mechanical properties whenever the sample is located inside the parametric domain and a poor prediction in the opposite case. This can be seen from the distribution of blue and red points with respect to the diagonal line that represents the perfect prediction, *i.e.*, the blue points are situated closer to the diagonal line than the red ones. Furthermore, the same conclusions can be extracted from figures 9a and 10a where the predicted values by s-PGD and the ones obtained by FEM for $\overline{E}_1$ are plotted as a function of two parameters. Again, s-PGD shows a good agreement between the predicted and the reference solution when the parameters values are taken in the center. On the contrary, a significant divergence is noticed when the minimum value of each parameter is considered.

Since we are dealing with linear elastic behavior, the generation of the database in the *offline* phase can be an expensive task, not because of the FEM calculations but rather due to the creation of the geometry and mesh of the unit-cells. However, as entailed in Table 2, this model requires around 200 unit-cells, which are considered costly for database generation, regarding

the error produced for each component at the test dataset (more than 10%).

In conclusion, the s-PGD model seems to be not totally able to well approximate the parametric solution of the overall mechanical properties of woven composite, in particular, when the parameters vary along the boundary. This can be attributed to the fact that this model fails in extrapolating the pre-calculated solutions. In addition, ensuring accurate results by the proposed model may be obtained by using more sampling points located closer to the domain boundary.

3.3. Macroscopic properties predicted by ANOVA-PGD

In this subsection, the results obtained by ANOVA-PGD are presented. Figure 8 shows an excellent agreement between the predicted and reference values of the orthotropic mechanical properties. Moreover, as shown in Table 2, using only 1045 pre-computed solutions and 25 unit-cells, the proposed method produces less error compared with the previous methods. Furthermore, from figures 9d and 10d, we notice that the current method provides a better approximation of the component $\overline{E}_1$ in the whole parametric domain.

Overall, it can be deduced from the findings that ANOVA-PGD permits to achieve more accurate predictions of the mechanical properties of woven composite using a limited dataset. It represents the right trade-off between precision and database volume. This can be explained by the ability of this method to consider sampling points in the volume as well as on the surface of the parametric domain.

As presented earlier, this parametric solution is approximated in two steps. First, an anchored-ANOVA decomposition is implemented using 21 sampling points. The latter have been generated by setting all parameters at

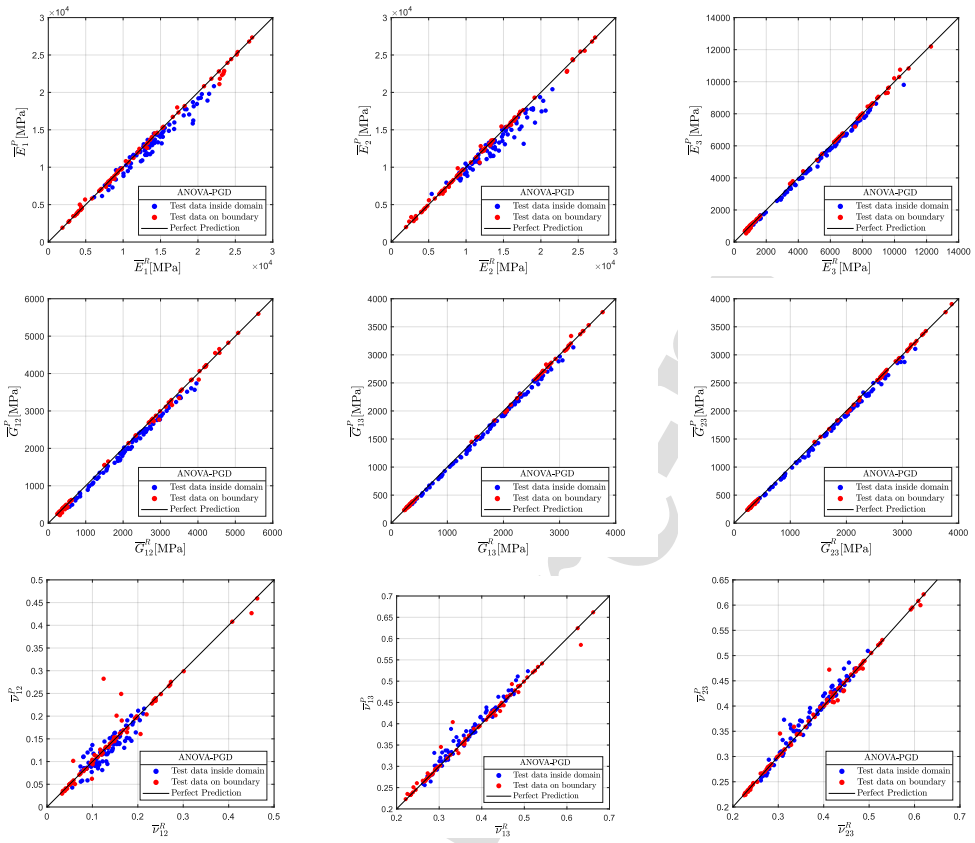

Figure 8: Scatterplots of predicted versus reference values of the mechanical properties of plain weave fabric composite using ANOVA-PGD. The red and blue points represent the test datasets on boundary and inside the parametric domain, respectively. While the diagonal line indicate the perfect prediction.

the center of the domain and varying, each time, one parameter between the maximum and minimum value. In each dimension, three sample points are used, in which the anchor point is included, to determine the one-dimensional functions using a polynomial interpolation technique such as spline interpolation or Lagrange interpolation, etc. Afterwards, the approximate solution is improved now by approximating the residual. In (Sancarlos et al., 2021a),

Table 2: Number of samples (number of finite element calculations) and unit-cells used to approximate the macroscopic properties of woven composite by non-intrusive PGD techniques and the error obtained in the test data set for each of these techniques..

non-intrusive	Number of	Number of				Errors	(E_{rr})				
PGD	Samples	unit cell	$\overline{E}_1$	$\overline{E}_2$	$\overline{E}_3$	$\overline{G}_{12}$	$\overline{G}_{13}$	$\overline{G}_{23}$	$\overline{\nu}_{12}$	$\overline{\nu}_{13}$	$\overline{\nu}_{23}$
SSL (level 0)	1024	16	0.11	0.12	0.04	0.04	0.03	0.03	0.18	0.06	0.06
SSL (level 1)	6144	48	0.11	0.12	0.04	0.03	0.03	0.03	0.14	0.05	0.05
s-PGD	200	200	0.1	0.21	0.1	0.31	0.22	0.09	0.39	0.05	0.06
ANOVA-PGD	1045	25	0.05	0.06	0.03	0.03	0.02	0.02	0.13	0.03	0.03

it is proposed to approximate this residual through non-intrusive PGD such as s-PGD. Here, the SSL level 0 has been chosen to construct this approximation trying to obtain excellent predictions for the points involved along the boundary of the parametric domain as presented in the previous subsection.

Summarizing, the following outcomes and key points can be derived:

- ANOVA-PGD model is appropriate for the presented problem since it requires a few dozen of unit cells and a few hundred of FE computations, to achieve a good approximation.

- s-PGD fails to well approximate the solution along the domain's boundary. Also, it uses a huge number of unit cells to build the database in contrast to other presented methods.

- SSL brings about significant errors inside the parametric domain for the first two hierarchical levels. It requires a huge number of precomputed solutions in order to reach an accuracy comparable to that of ANOVA-PGD. However, improving the approximation level leads to

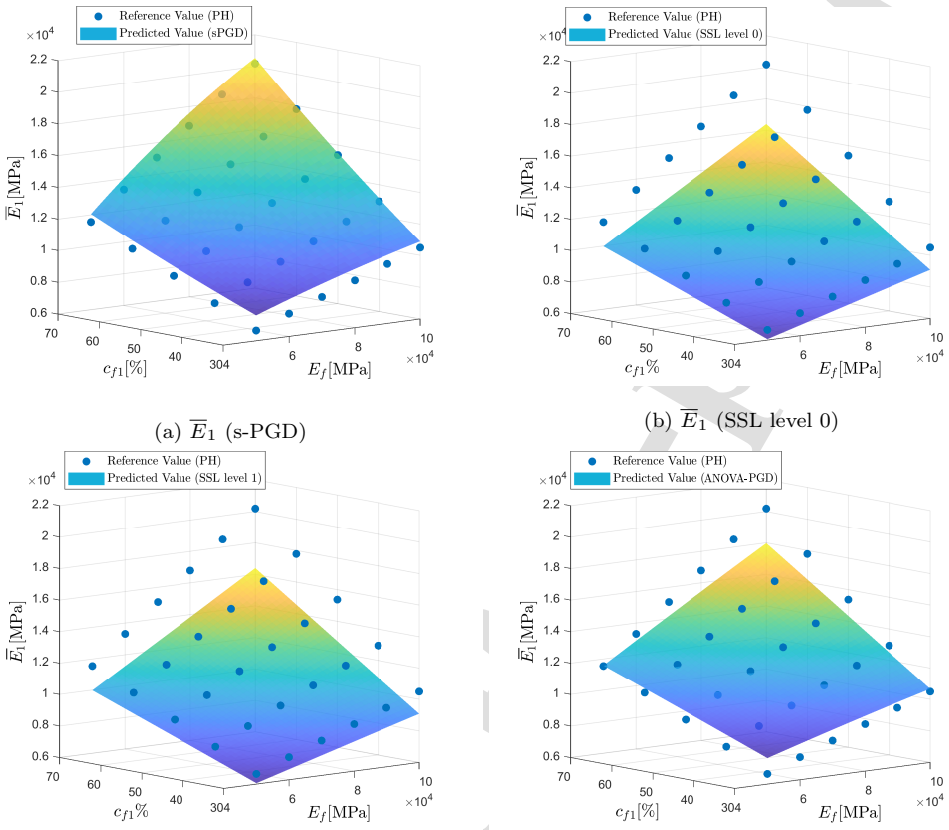

(a) $\overline{E}_1$ (s-PGD)

(b) $\overline{E}_1$ (SSL level 0)

(c) $\overline{E}_1$ (SSL level 1)

(d) $\overline{E}_1$ (ANOVA-PGD)

Figure 9: Comparison between reference and predicted values of longitudinal modulus $\overline{E}_1$, as a function of fibre Young's modulus E_f and intra-weft fibre volume fraction c_{f1}. With $a_1 = 2$ mm, $a_2 = 2$ mm, $h = 0.3$ mm, $c = 0.2$ mm, $c_{f2} = 50\%$ $v_f = 0.3$, $E_m = 2074$ MPa, $v_m = 0.3$ are chosen **inside** the parametric domain. (a) the values predicted by s-PGD. (b) Values predicted by SSL level 0. (c) Values predicted by SSL level 1. (d) Values predicted by ANOVA-PGD.

an exponential increase in the number of samples as well as the unit cell generations.

.

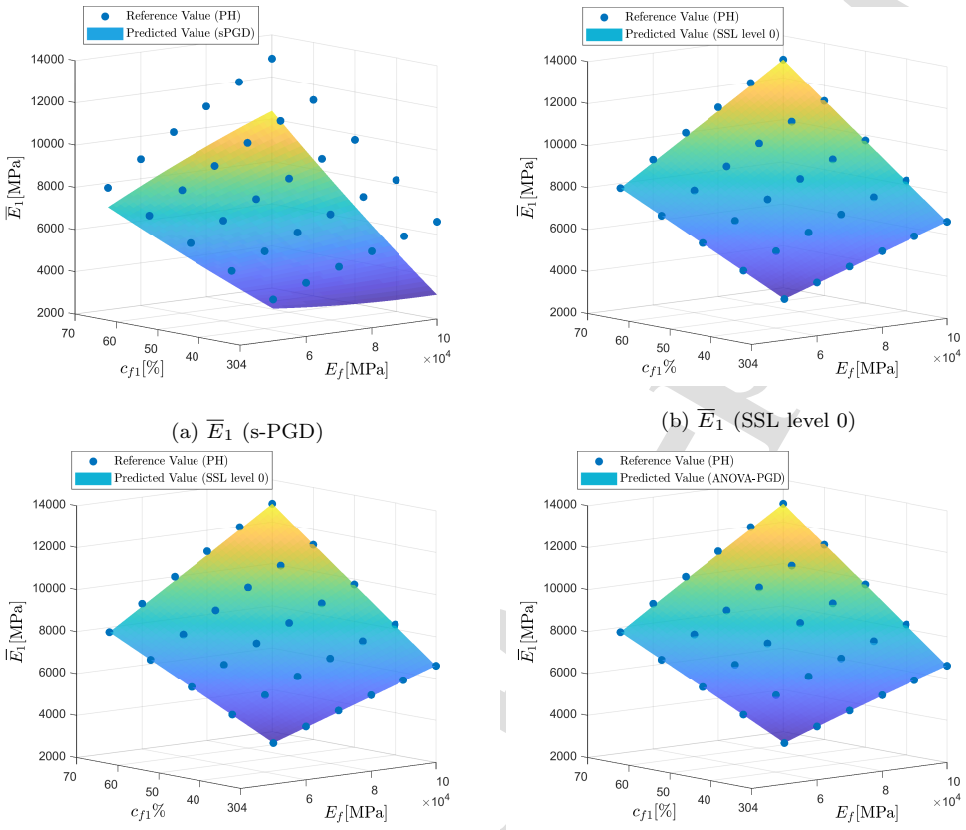

(a) $\overline{E}_1$ (s-PGD)

(b) $\overline{E}_1$ (SSL level 0)

(c) $\overline{E}_1$ (SSL level 1)

(d) $\overline{E}_1$ (ANOVA-PGD)

Figure 10: Comparison between reference and predicted values of longitudinal modulus $\overline{E}_1$, as a function of fibre Young's modulus E_f and intra-weft fibre volume fraction c_{f1}. With $a_1 = 0.8$ mm, $a_2 = 0.8$ mm, $h = 0.2$ mm, $c = 0.1$ mm, $c_{f2} = 30\%$, $v_f = 0.2$, $E_m = 500$ MPa, $v_m = 0.2$ are chosen on the **boundary** of the domain. (a) The values predicted by s-PGD. (b) Values predicted by SSL level 0. (c) Values predicted by SSL level 1. (d) Values predicted by ANOVA-PGD.

4. Conclusions and perspectives

In this study, non-intrusive PGD-based methods have been applied to construct a multiparametric approximation of the macroscopic properties of

plain weave composite including various microstructural parameters. These methods allow for advanced parametric analyses, considering the parameters as extra-coordinates of the problem, while circumventing the resulting *curse of dimensionality* by using the separated representation form of the solution. To achieve a good prediction of the mechanical properties for plain weave, based on limited number of *offline* computations, a thorough comparative analysis of three non-intrusive PGD formulations, SSL, s-PGD and ANOVA-PGD, is presented. Therefore, the following concluding remarks can be outlined:

- ANOVA-PGD provides efficient and accurate predictions of the homogenized properties of plain weave composites both inside the 10-dimensional parameter space, and at its boundary.
- This technique well approximates the multi-parametric solution using a reduced number of high-fidelity solutions and related microstructures in the *offline* stage, compared to the other presented non-intrusive PGD techniques.
- The same formulation has been successfully applied to approximate the multiparametric solution for other balanced weave reinforcement architectures including 2/2 Twill weave and 5H Satin weave pattern, as well as for unbalanced weave architecture such as 2/3 Twill weave pattern.
- A Graphical User Interface application (GUI) has been created using Matlab App Designer as shown in Figure 11. This application can

be easily employed by designers and engineers to deduce, instantaneously, the macroscopic properties of woven composite for any given set of microstructural parameters by setting cursors and without any microstructure generation and FE computation using periodic homogenization. Such a tool allows hence assessing in real-time the influence of the input parameters on the overall composite behavior. It can be also employed as a decision-making tool towards optimal material selection.

The results presented in this work make non-intrusive PGD-based formulations a promising technique for solving high-dimensional parametric solutions of many engineering problems of composites using a limited dataset, especially, where a huge database is impossible or difficult to build. This research has focused on studying the linear elastic properties of woven fabric composites taking into account geometrical and material parameters. There are many opportunities for future works, for instance, by incorporating more parameters, including yarn angle and total fibre volume fraction, or by investigating other types of composites such as the 3D woven composites (interlock woven fabric composite). This work could also be extended to build subsequent virtual abacuses and vademecums dealing with nonlinear behaviors including viscoelasticity, viscoplasticity, and damage (Praud et al., 2017a, 2021b; Kriaa et al., 2020).

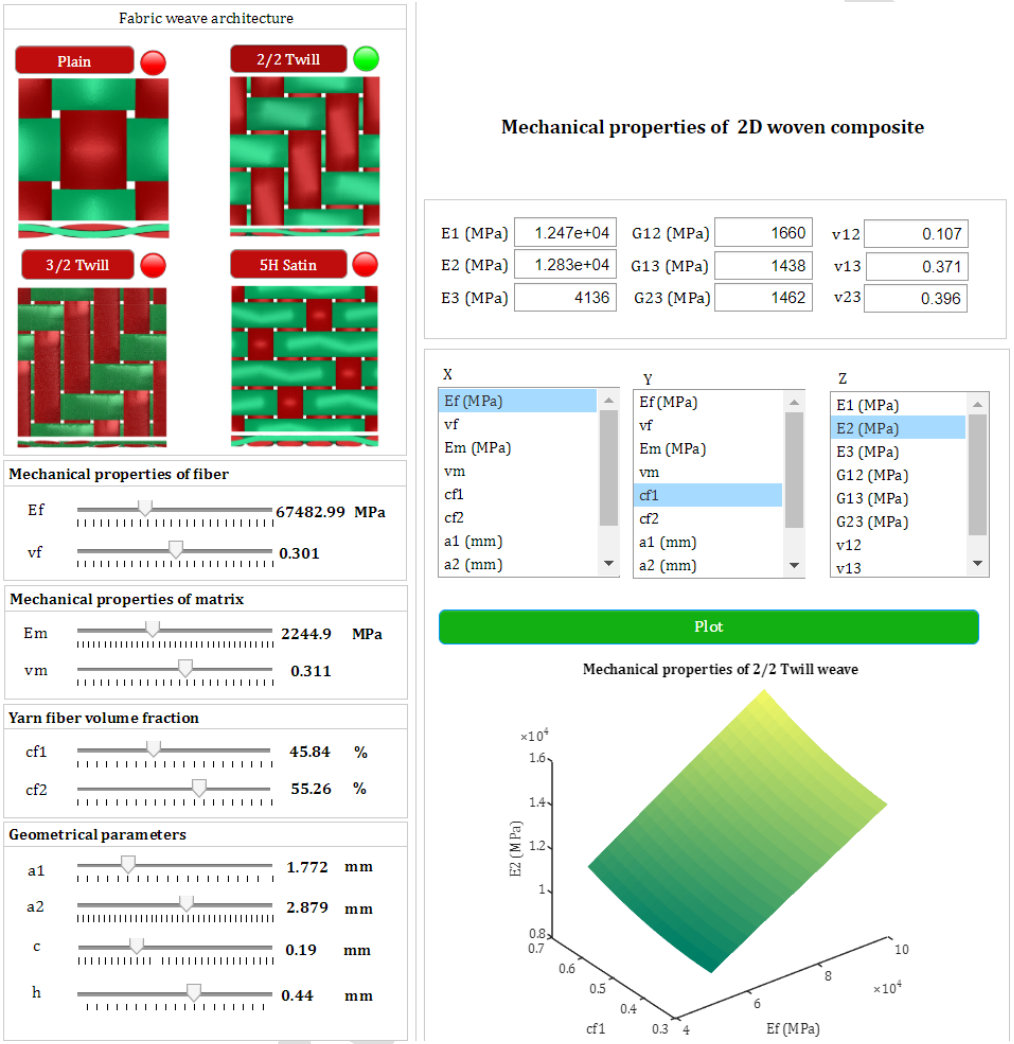

Figure 11: Graphical User Interface application (GUI) for real-time evaluation of the homogenized properties of 2D woven composites (Plain weave, 2/2 Twill weave, 3/2 Twill weave and 5H Satin weave) involving microstructure geometry and material properties of its constituents.

References

Ammar, A., Huerta, A., Chinesta, F., Cueto, E., Leygue, A., 2014. Parametric solutions involving geometry: a step towards efficient shape opti-

mization. Computer Methods in Applied Mechanics and Engineering 268, 178–193.

Ammar, A., Mokdad, B., Chinesta, F., Keunings, R., 2006. A new family of solvers for some classes of multidimensional partial differential equations encountered in kinetic theory modeling of complex fluids. Journal of non-Newtonian fluid Mechanics 139, 153–176.

Ammar, A., Mokdad, B., Chinesta, F., Keunings, R., 2007. A new family of solvers for some classes of multidimensional partial differential equations encountered in kinetic theory modelling of complex fluids: Part ii: Transient simulation using space-time separated representations. Journal of non-newtonian fluid mechanics 144, 98–121.

Barral, M., Chatzigeorgiou, G., Meraghni, F., Léon, R., 2020. Homogenization using modified mori-tanaka and tfa framework for elastoplastic-viscoelastic-viscoplastic composites: Theory and numerical validation. International Journal of Plasticity 127, 102632.

Borzacchiello, D., Aguado, J.V., Chinesta, F., 2019. Non-intrusive sparse subspace learning for parametrized problems. Archives of Computational Methods in Engineering 26, 303–326.

Brisard, S., Dormieux, L., 2010. Fft-based methods for the mechanics of composites: A general variational framework. Computational Materials Science 49, 663–671.

Chatzigeorgiou, G., Charalambakis, N., Chemisky, Y., Meraghni, F., 2016. Periodic homogenization for fully coupled thermomechanical modeling of

dissipative generalized standard materials. International Journal of Plasticity 81, 18–39.

Chatzigeorgiou, G., Meraghni, F., Charalambakis, N., 2022. Multiscale Modeling Approaches for Composites. Elsevier. URL: https://www.sciencedirect.com/science/article/pii/B9780128231432000084, doi:https://doi.org/10.1016/B978-0-12-823143-2.00008-4.

Chen, Q., Chatzigeorgiou, G., Robert, G., Meraghni, F., 2022. Viscoelastic-viscoplastic homogenization of short glass-fiber reinforced polyamide composites (pa66/gf) with progressive interphase and matrix damage: New developments and experimental validation. Mechanics of Materials 164, 104081.

Chen, Q., Wang, G., Chen, X., 2018. Three-dimensional parametric finite-volume homogenization of periodic materials with multi-scale structural applications. International Journal of Applied Mechanics 10, 1850045.

Chinesta, F., Ammar, A., Cueto, E., 2010. Recent advances and new challenges in the use of the proper generalized decomposition for solving multidimensional models. Archives of Computational methods in Engineering 17, 327–350.

Chinesta, F., Ammar, A., Leygue, A., Keunings, R., 2011a. An overview of the proper generalized decomposition with applications in computational rheology. Journal of Non-Newtonian Fluid Mechanics 166, 578–592.

Chinesta, F., Ladeveze, P., Cueto, E., 2011b. A short review on model

order reduction based on proper generalized decomposition. Archives of Computational Methods in Engineering 18, 395–404.

Chinesta, F., Leygue, A., Bordeu, F., Aguado, J.V., Cueto, E., González, D., Alfaro, I., Ammar, A., Huerta, A., 2013. Pgd-based computational vademecum for efficient design, optimization and control. Archives of Computational Methods in Engineering 20, 31–59.

Courard, A., Néron, D., Ladevèze, P., Ballere, L., 2016. Integration of pgd-virtual charts into an engineering design process. Computational Mechanics 57, 637–651.

Erol, O., Powers, B.M., Keefe, M., 2017. Effects of weave architecture and mesoscale material properties on the macroscale mechanical response of advanced woven fabrics. Composites Part A: Applied Science and Manufacturing 101, 554–566.

Eshelby, J.D., 1957. The determination of the elastic field of an ellipsoidal inclusion, and related problems. Proceedings of the royal society of London. Series A. Mathematical and physical sciences 241, 376–396.

Germoso, C., Quaranta, G., Duval, J.L., Chinesta, F., 2020. Non-intrusive in-plane-out-of-plane separated representation in 3d parametric elastodynamics. Computation 8, 78.

Hallal, A., Younes, R., Fardoun, F., 2013. Review and comparative study of analytical modeling for the elastic properties of textile composites. Composites Part B: Engineering 50, 22–31.

Hill, R., 1965. A self-consistent mechanics of composite materials. Journal of the Mechanics and Physics of Solids 13, 213–222.

Hill, R., 1967. The essential structure of constitutive laws for metal composites and polycrystals. Journal of the Mechanics and Physics of Solids 15, 79–95.

Ibáñez, R., Abisset-Chavanne, E., Ammar, A., González, D., Cueto, E., Huerta, A., Duval, J.L., Chinesta, F., 2018. A multidimensional data-driven sparse identification technique: the sparse proper generalized decomposition. Complexity 2018.

Kamiński, M., 1999. Boundary element method homogenization of the periodic linear elastic fiber composites. Engineering Analysis with Boundary Elements 23, 815–823.

Kriaa, Y., Ammar, A., Zouari, B., 2020. Data-driven model based on the simulation of cracking process in brittle material using the phase-field method in application. Comptes Rendus. Mécanique 348, 729–744.

Kumar, R.S., 2013. Textiles for industrial applications. CRC Press.

Leon, A., Mueller, S., de Luca, P., Said, R., Duval, J.L., Chinesta, F., 2019. Non-intrusive proper generalized decomposition involving space and parameters: application to the mechanical modeling of 3d woven fabrics. Advanced Modeling and Simulation in Engineering Sciences 6, 1–20.

Liang, B., Zhang, W., Fenner, J.S., Gao, J., Shi, Y., Zeng, D., Su, X., Liu, W.K., Cao, J., 2019. Multi-scale modeling of mechanical behavior of

cured woven textile composites accounting for the influence of yarn angle variation. Composites Part A: Applied Science and Manufacturing 124, 105460.

Liang, B., Zhang, W., Gao, S., 2020. Analysis of the influence of yarn angle on the mechanical behaviors of cured woven composites. High Performance Polymers 32, 975–983.

Lin, H., Brown, L.P., Long, A.C., 2011. Modelling and simulating textile structures using texgen, in: Advanced Materials Research, Trans Tech Publ. pp. 44–47.

Long, A.C., 2006. Design and manufacture of textile composites. CRC press.

Lu, Y., Blal, N., Gravouil, A., 2018. Multi-parametric space-time computational vademecum for parametric studies: Application to real time welding simulations. Finite Elements in Analysis and Design 139, 62–72.

Mercier, S., Molinari, A., 2009. Homogenization of elastic–viscoplastic heterogeneous materials: Self-consistent and mori-tanaka schemes. International Journal of Plasticity 25, 1024–1048.

Michel, J.C., Moulinec, H., Suquet, P., 1999. Effective properties of composite materials with periodic microstructure: a computational approach. Computer methods in applied mechanics and engineering 172, 109–143.

Miqoi, N., Pomarede, P., Meraghni, F., Declercq, N.F., Guillaumat, L., Le Coz, G., Delalande, S., 2021. Detection and evaluation of barely visible

impact damage in woven glass fabric reinforced polyamide 6.6/6 composite using ultrasonic imaging, x-ray tomography and optical profilometry. International Journal of Damage Mechanics 30, 323–348.

Mori, T., Tanaka, K., 1973. Average stress in matrix and average elastic energy of materials with misfitting inclusions. Acta metallurgica 21, 571–574.

Mura, T., 2013. Micromechanics of defects in solids. Springer Science & Business Media.

Nemat-Nasser, S., Hori, M., 2013. Micromechanics: overall properties of heterogeneous materials. Elsevier.

Praud, F., 2018. Multi-scale modelling of thermoplastic-based woven composites, cyclic and time-dependent behaviour. Ph.D. thesis. Paris, ENSAM.

Praud, F., Chatzigeorgiou, G., Bikard, J., Meraghni, F., 2017a. Phenomenological multi-mechanisms constitutive modelling for thermoplastic polymers, implicit implementation and experimental validation. Mechanics of Materials 114, 9–29.

Praud, F., Chatzigeorgiou, G., Chemisky, Y., Meraghni, F., 2017b. Hybrid micromechanical-phenomenological modelling of anisotropic damage and anelasticity induced by micro-cracks in unidirectional composites. Composite Structures 182, 223–236.

Praud, F., Chatzigeorgiou, G., Meraghni, F., 2021a. Fully integrated multi-scale modelling of damage and time-dependency in thermoplastic-based

woven composites. International Journal of Damage Mechanics 30, 163–195.

Praud, F., Schmitt, T., Zabeida, O., Maïza, S., Martinu, L., Lévesque, M., 2021b. Phase field fracture models to predict crack initiation and propagation in anti-reflective coatings. Thin Solid Films 736, 138920.

Sancarlos, A., Champaney, V., Duval, J.L., Cueto, E., Chinesta, F., 2021a. Pgd-based advanced nonlinear multiparametric regressions for constructing metamodels at the scarce-data limit. arXiv preprint arXiv:2103.05358 .

Sancarlos, A., Ghnatios, C., Duval, J.L., Zerbib, N., Cueto, E., Chinesta, F., 2021b. Fast computation of multi-parametric electromagnetic fields in synchronous machines by using pgd-based fully separated representations. Energies 14, 1454.

de Sousa Vieira, C., Marques, S.P.C., 2019. A new three-dimensional finite-volume model for evaluation of thermal conductivity of periodic multiphase composites. International Journal of Heat and Mass Transfer 139, 412–424.

Tikarrouchine, E., Benaarbia, A., Chatzigeorgiou, G., Meraghni, F., 2021. Non-linear fe2 multiscale simulation of damage, micro and macroscopic strains in polyamide 66-woven composite structures: analysis and experimental validation. Composite Structures 255, 112926.

Tikarrouchine, E., Chatzigeorgiou, G., Chemisky, Y., Meraghni, F., 2019. Fully coupled thermo-viscoplastic analysis of composite structures by

means of multi-scale three-dimensional finite element computations. International Journal of Solids and Structures 164, 120–140.

Tikarrouchine, E., Chatzigeorgiou, G., Praud, F., Piotrowski, B., Chemisky, Y., Meraghni, F., 2018. Three-dimensional fe2 method for the simulation of non-linear, rate-dependent response of composite structures. Composite Structures 193, 165–179.

Verpoest, I., Lomov, S.V., 2005. Virtual textile composites software wisetex: Integration with micro-mechanical, permeability and structural analysis. Composites Science and Technology 65, 2563–2574.

Wang, B., Fang, G., Liu, S., Fu, M., Liang, J., 2018. Progressive damage analysis of 3d braided composites using fft-based method. Composite Structures 192, 255–263.

Zhou, G., Sun, Q., Meng, Z., Li, D., Peng, Y., Zeng, D., Su, X., 2021. Experimental investigation on the effects of fabric architectures on mechanical and damage behaviors of carbon/epoxy woven composites. Composite structures 257, 113366.

Zou, X., Conti, M., Díez, P., Auricchio, F., 2018. A nonintrusive proper generalized decomposition scheme with application in biomechanics. International Journal for Numerical Methods in Engineering 113, 230–251.

Highlights:

- Effective stiffness prediction for composite having different woven-fabric architectures and microstructure parameters without any microstructure generation and meshing nor FE computations using periodic homogenization.
- Comparative analysis of three non-intrusive PGD formulations (SSL, sPGD and ANOVA-PGD) in terms of accuracy and robustness.
- The ANOVA-PGD technique is proving to be the best compromise between the cost of generating the database and the accuracy of the approximation of the stiffness over the entire parameter space.
- Creation of a Graphical User Interface application (GUI) aimed at predicting in real-time the effect of the microstructure parameters on the macroscopic properties of different woven-fabric architectures.

AUTHORSHIP STATEMENT Manuscript title:

Multi-parametric modelling of composite materials based on non-intrusive PGD informed by multi-scale analyses: application for real-time stiffness prediction of woven composites

M. El Fallaki Idrissi: Writing - Original Draft, Formal Analysis, Investigation, Methodology, Validation

F. Praud: Review & Editing, Conceptualization, Investigation

V. Champaney: Review & Editing, Formal Analysis, Investigation, Methodology

F. Chinesta: Conceptualization, Methodology, Formal Analysis, Investigation, Review & Editing.

F. Meraghni: Conceptualization, Methodology, Formal Analysis, Investigation, Review & Editing, Project administration

Declaration of interests

☒ The authors declare that they have no known competing financial interests or personal relationships that could have appeared to influence the work reported in this paper.

☐The authors declare the following financial interests/personal relationships which may be considered as potential competing interests: